JOURNAL OF VIROLOGY, Jan. 2003, p. 84–96 Vol. 77, No. 1
0022-538X/03/$08.00+0 DOI: 10.1128/JVI.77.1.84–96.2003

Sequences Downstream of the 5′ Splice Donor Site Are Required for both Packaging and Dimerization of Human Immunodeficiency Virus Type 1 RNA

Rodney S. Russell,[1,2] Jing Hu,[1] Véronique Bériault,[1,2] Andrew J. Mouland,[1,2,3] Lawrence Kleiman,[1,2] Mark A. Wainberg,[1,2,3]* and Chen Liang[1,3]*

McGill AIDS Centre, Lady Davis Institute-Jewish General Hospital, Montreal, Quebec H3T 1E2,[1] and Departments of Medicine[3] and Microbiology and Immunology,[2] McGill University, Montreal, Quebec H3A 2B4, Canada

Received 18 April 2002/Accepted 27 September 2002

Two copies of human immunodeficiency virus type 1 RNA are incorporated into each virus particle and are further converted to a stable dimer as the virus particle matures. Several RNA segments that flank the 5′ splice donor site at nucleotide (nt) 289 have been shown to act as packaging signals. Among these, RNA stem-loop 1 (SL1) (nt 243 to 277) can trigger RNA dimerization through a "kissing-loop" mechanism and thus is termed the dimerization initiation site. However, it is unknown whether other packaging signals are also needed for dimerization. To pursue this subject, we mutated stem-loop 3 (SL3) (nt 312 to 325), a GA-rich region (nt 325 to 336), and two G-rich repeats (nt 363 to 367 and nt 405 to 409) in proviral DNA and assessed the effects on RNA dimerization by performing native Northern blot analyses. Our results show that the structure but not the specific RNA sequence of SL3 is needed not only for efficient viral RNA packaging but also for dimerization. Mutations of the GA-rich sequence severely diminished viral RNA dimerization as well as packaging; the combination of mutations in both SL3 and the GA-rich region led to further decreases, implying independent roles for each of these two RNA motifs. Compensation studies further demonstrated that the RNA-packaging and dimerization activity of the GA-rich sequence may not depend on a putative interaction between this region and a CU repeat sequence at nt 227 to 233. In contrast, substitutions in the two G-rich sequences did not cause any diminution of viral RNA packaging or dimerization. We conclude that both the SL3 motif and GA-rich RNA sequences, located downstream of the 5′ splice donor site, are required for efficient RNA packaging and dimerization.

Human immunodeficiency virus type 1 (HIV-1) contains a diploid RNA genome that is noncovalently associated in dimer form at its 5′ ends in a parallel orientation. These attached viral RNA regions were first described as the dimer linkage structure in monkey sarcoma virus (18), and this term has been used subsequently to describe dimerization in other retroviruses. Two models have been proposed to illustrate molecular interactions that constitute the HIV-1 dimer linkage structure. The first involves a tetra-stranded RNA structure, termed a G-tetrad, that is formed by G-rich RNA sequences (23). This structure has been implicated in maintaining the integrity of chromosome telomeres in which stretches of G-rich nucleotide sequences are present (12). G-rich RNA regions were also identified at the 5′ end of HIV-1 RNA downstream of the major splice donor site. It was therefore hypothesized that formation of G-tetrad structures may contribute to the maintenance of RNA dimers; this notion has been supported by studies performed with synthetic viral RNA fragments, yet has not been extensively tested in the context of the full-length viral RNA genome (2, 13, 23, 42).

The second model involves a "kissing-loop" mechanism and is derived from the observation that the stem-loop 1 (SL1) RNA segment, located upstream of the 5′ splice donor site, was able to spontaneously form dimers under appropriate buffer conditions (19, 28). This reaction is believed to be initiated by the SL1 loop palindrome sequence (e.g., 5′-GCGCG C-3′ in HXB2D) via the formation of regular Watson-Crick base pairs; SL1 was thus termed the dimerization initiation site (31, 34, 41). Subsequent studies demonstrated that both the palindrome and the stem are essential for the dimerization activity of SL1 (7, 9, 20, 31). However, substantial amounts of dimerized RNA were detected in mutant viruses containing altered loop sequences or a disrupted SL1 stem structure (3, 35); thus, SL1 may constitute only part of the dimer linkage structure.

The dimer linkage structure of HIV-1 overlaps the RNA packaging signals. Stem-loop 3 (SL3) and its flanking RNA sequences, together with SL1, represent major packaging signals (5). In addition to the well-documented roles of SL1 in RNA dimerization, cell-free assays with synthetic RNA molecules showed that an antisense nucleotide oligomer that binds to SL3 and a downstream GA-rich RNA region was able to inhibit RNA dimerization (43).

In the present study, we have addressed this subject in vivo by mutating relevant RNA sequences in proviral DNA and analyzing virion-derived mutant RNAs by native Northern blotting. Our data show that both SL3 and the GA-rich RNA segments are required for both RNA packaging and dimerization.

* Corresponding author. Mailing address: McGill AIDS Centre, Lady Davis Institute-Jewish General Hospital, 3755 Cote Ste-Catherine Rd., Montreal, Quebec, Canada H3T 1E2. Phone: (514) 340-8260. Fax: (514) 340-7537. E-mail: chen.liang@mcgill.ca; mark.wainberg@mcgill.ca.

MATERIALS AND METHODS

Plasmid construction. Infectious HIV-1 cDNA clone BH10 was employed to generate the constructs described below, and all mutations were introduced by PCR-based strategies with the *Pfu* enzyme (Stratagene, La Jolla, Calif.). MD1, MD2, and MD3 are deletion mutations that were engineered by PCR with primer pair pBssH-S (5′-CTGAAGCGCGCACGGCAAGAGG-3′ [nt 252 to 273]) and pD1 (5′-CCATCTCTCTCCTTCTAGCGCTAGTCAAAATTTTTGGC-3′ [nt 339 to 298]), pBssH-S and pD2 (5′-GCTCTCGCACCCATCTCTTTCTAGCCTCCGC-3′ [nt 349 to 315]), and pBssH-S and pD3 (5′-GCTCTCGCACCCATCTCTTTCTAGCGCTAGTCAAAATTTTTGGC-3′ [nt 349 to 298]), respectively (Fig. 1). The PCR products were then used as primers together with pSph-A (5′-GGCCCTGCATGCACTGGATGC-3′ [nt 1000 to 980]) in a second round of PCR. Final PCR products were digested with the restriction enzymes *Bss*HII and *Sph*I and inserted into BH10.

Constructs MS1 to MS6, MG1, MG2, and MG12 contain substitutions (Fig. 1) and were generated with similar strategies with primers pS1 (5′-CCATCTCTCTCCTTCTAGCTAGCGCTAGTCAAAATTTTTGGC-3′ [nt 339 to 298]), pS2 (5′-GCTCTCGCACCCATCTCTGATGTTCTAGCCTCCGC-3′ [nt 349 to 315]), pS3 (5′-GCTCTCGCACCCATCTCTGATGTTCTAGCTAGCGCTAGTCAAAATTTTTGGC-3′ [nt 349 to 298]), pS4 (5′-CTCTCTCCTTCTAGCCTCCTTGTCTCAAAATTTTTGGCGTAC-3′ [nt 335 to 294]), pS5 (5′-GCACCCATCTCTCTCCTTGACAACTCCTTGTCTCAAAATTTTTGGCGTAC-3′ [nt 349 to 294]), pS6 (5′-CGCTCTCGCACCCATATGTCTCCTTCTAGCCTC-3′ [nt 350 to 318]), pG1 (5′-CCATCGATCTAATTCACCGCCGCTTAATACTGACGC-3′ [nt 383 to 348]), and pG2 (5′-TAATTTATATTTTTTCTTACCGCCTGGCCTTAACCG-3′ [nt 428 to 393]), respectively (Fig. 1).

BH-GA contains a substitution of a 5′-CTCTCTC-3′ (nt 227 to 233) by the sequence 5′-AGAG-3′ (see Fig. 6A) and was generated as described previously (24). Construct MS7 was designed to contain a compensatory mutation for the MS6 mutant and was generated with primer MS6C-A (5′-CCTGCGTCGACATAGCTCCTCTGG-3′ [nt 241 to 218]) in combination with primer U5-1S (5′-GAGATCCCTCAGACCCTTTTAG-3′ [nt 137 to 158]), with the MS6 construct as a template. The PCR product was then used as a primer together with pSph-A in a second round of PCR, and the final PCR products were digested with *Nar*I and *Sph*I and inserted into BH10.

To generate an antisense riboprobe to be used in RNase protection assays, a 486-bp fragment was amplified from the BH10 proviral DNA sequence with primer pair RPA-S (5′-CAgggcccGAGAGCTGCATCCGGAG-3′ [nt −164 to −140]), which was modified to contain an *Apa*I restriction enzyme site (shown in lowercase letters), and RPA-A (5′-CCTCCGgaattcAAAATTTTTGGCG-3′ [nt 321 to 297]), which was modified to contain an *Eco*RI restriction enzyme site (shown in lowercase letters). The resulting PCR product was digested with *Apa*I and *Eco*RI and inserted into the pBluescript II KS$^+$ cloning vector (Stratagene) that had been cut with the same enzymes to generate construct RPA1.

Cell culture, transfection, and infection. COS-7, MT-2, and Jurkat cells were grown in Dulbecco's modified Eagle's medium and RPMI 1640 medium, respectively, both supplemented with 10% fetal calf serum. Transfection of COS-7 cells was performed with Lipofectamine (Invitrogen, Burlington, Ontario, Canada). Quantities of progeny viruses were determined by measuring levels of p24 antigen with an enzyme-linked immunosorbent assay (Vironostika HIV-1 Antigen Microelisa System; Organon Teknika Corporation, Durham, N.C.).

MT-2 or Jurkat cells (5×10^5) were incubated with aliquots of viruses equivalent to 5 ng of p24 in 2 ml of medium at 37°C for 2 h. The cells were then washed twice and maintained in 10 ml of medium. Culture fluids were collected at various times to determine levels of reverse transcriptase activity.

Native Northern blotting. Progeny viruses generated by transfected COS-7 cells were first clarified by centrifugation in a Beckman GR-6S centrifuge at 3,000 rpm for 30 min at 4°C and then pelleted through a 20% sucrose cushion by ultracentrifugation in a Beckman XL-80 ultracentrifuge with an SW41 rotor at 40,000 rpm for 1 h at 4°C. Virus pellets were suspended in 300 μl of TN buffer (50 mM Tris-HCl [pH 7.8], 10 mM NaCl); a 2-μl portion was removed for p24 determination, and the remaining viruses were treated with virus lysis buffer (50 mM Tris-HCl [pH 7.4], 10 mM EDTA, 1% sodium dodecyl sulfate, 100 mM NaCl, 50 μg of yeast tRNA/ml, 100 μg of proteinase K/ml) for 20 min at 37°C. Samples were then extracted twice with phenol-chloroform-isoamyl alcohol (25:24:1) and once with chloroform.

Viral RNA was precipitated in 2.5 volumes of 95% ethanol. RNA pellets were washed with 70% ethanol and dissolved in TE (Tris-EDTA) buffer. An amount of viral RNA equivalent to 150 ng of HIV-1 p24 was fractionated on 0.9% native agarose gels in 1× TBE (Tris-borate-EDTA) buffer at 100 V for 4 h at 4°C and analyzed by Northern blotting (38) with an [α-^{32}P]dCTP (ICN, Irvine, Calif.)-labeled 2-kb HIV-1 DNA fragment (nt 1 to 2000) as a probe. Bands were visualized by autoradiography and quantified by digital image analysis with the NIH Image program. To determine the thermostability of viral RNA dimers, RNA samples were incubated at various temperatures (25°C, 40°C, 45°C, 50°C, and 55°C) for 10 min in a buffer containing 100 mM NaCl before being separated on native agarose gels.

RNase protection assays. Preparation of riboprobes and RNase protection assay experiments were done based on previously described protocols (7, 8). Briefly, radiolabeled probes were in vitro transcribed from *Bsp*EI-linearized plasmid RPA1 with T7 RNA polymerase in the presence of [α-^{32}P]UTP (ICN, Irvine, Calif.). RNA was isolated from viruses as described above. Cytoplasmic RNA was isolated from transfected COS-7 cells by resuspending the cell pellets in 400 μl of cell lysis buffer (10 mM Tris-HCl [pH 7.4], 140 mM NaCl, 1.5 mM $MgCl_2$, 0.5% Nonidet P-40, 1 mM dithiothreitol, 100 U of RNase inhibitor [Invitrogen]), then incubated on ice for 5 min, and centrifuged at 13,000 rpm for 10 min at 4°C. Supernatants were treated with 0.2% sodium dodecyl sulfate and 125 μg of proteinase K per ml at 37°C for 20 min and then subjected to phenol-chloroform extraction and ethanol precipitation as described above.

Quantities of total cytoplasmic RNA were determined by spectrophotometry at 260 nm. Amounts of virion RNA equivalent to 25 ng of p24 capsid antigen or 250 ng of cytoplasmic RNA were treated with 10 U of DNase I (Invitrogen) for 30 min at 37°C to remove any plasmid contamination and then subjected to phenol-chloroform extraction and ethanol precipitation before analysis with the RNase protection assay II kit (Ambion Inc., Austin, Tex.). Briefly, the RNA was incubated at 42°C overnight with an excess of labeled riboprobe (10^5 cpm), followed by digestion with RNases specific for single-stranded RNA. Protected fragments were separated on 5% polyacrylamide–8 M urea gels, visualized by autoradiography, and quantified by digital image analysis with the NIH Image program.

RESULTS

SL3 is needed for both viral RNA packaging and dimerization. SL3 is known to be an important HIV-1 RNA packaging signal (1, 5, 7, 8, 15, 25, 30). To further assess the potential role of SL3 in viral RNA dimerization, we generated a series of mutations. Loop sequence 5′-GGAG-3′ (nt 317 to 320) was either deleted to create construct MD1 or replaced with a 5′-GCTA-3′ sequence to generate construct MS1 (Fig. 1); the latter sequence was designed so as not to disrupt the secondary structure of SL3 (Fig. 1B). Next, we destabilized the base pairs within the stem by changing the sequence 5′-CTAGC-3′ (nt 312 to 316) to 5′-GACAA-3′ in construct MS4 (Fig. 1). To restore the stem structure, the right portion of the stem sequence (5′-GCTAG-3′) (nt 321 to 325) was changed to 5′-TTGTC-3′ in construct MS5 (Fig. 1).

The various DNA clones were transfected into COS-7 cells, and the progeny viruses thus generated were used to infect MT-2 and Jurkat cells. Both of these cell lines are CD4$^+$ and thus are permissive for HIV-1 infection. The results shown in Fig. 2A show that the MD1 and MS4 mutations caused delays in virus growth in MT-2 cells; in contrast, the MS1 and MS5 mutants grew almost as well as the wild-type virus. Differences in levels of infectivity between mutant and wild-type viruses were further verified in Jurkat cells (Fig. 2B). Since HIV-1 grew with slower kinetics in Jurkat cells than in MT-2 cells, as observed in the growth curves of wild-type BH10, replication differences between wild-type and mutant viruses were more pronounced in the Jurkat system. The extent to which these four viruses were able to replicate was MS1 > MS5 > MS4 > MD1.

Viral RNA dimerization and packaging studies were performed on virus particles derived from transfection of nonpermissive COS-7 cells. We used these nonpermissive cells so as not to allow viral mutants to undergo reversions that might regularly occur over multiple rounds of infection during cul-

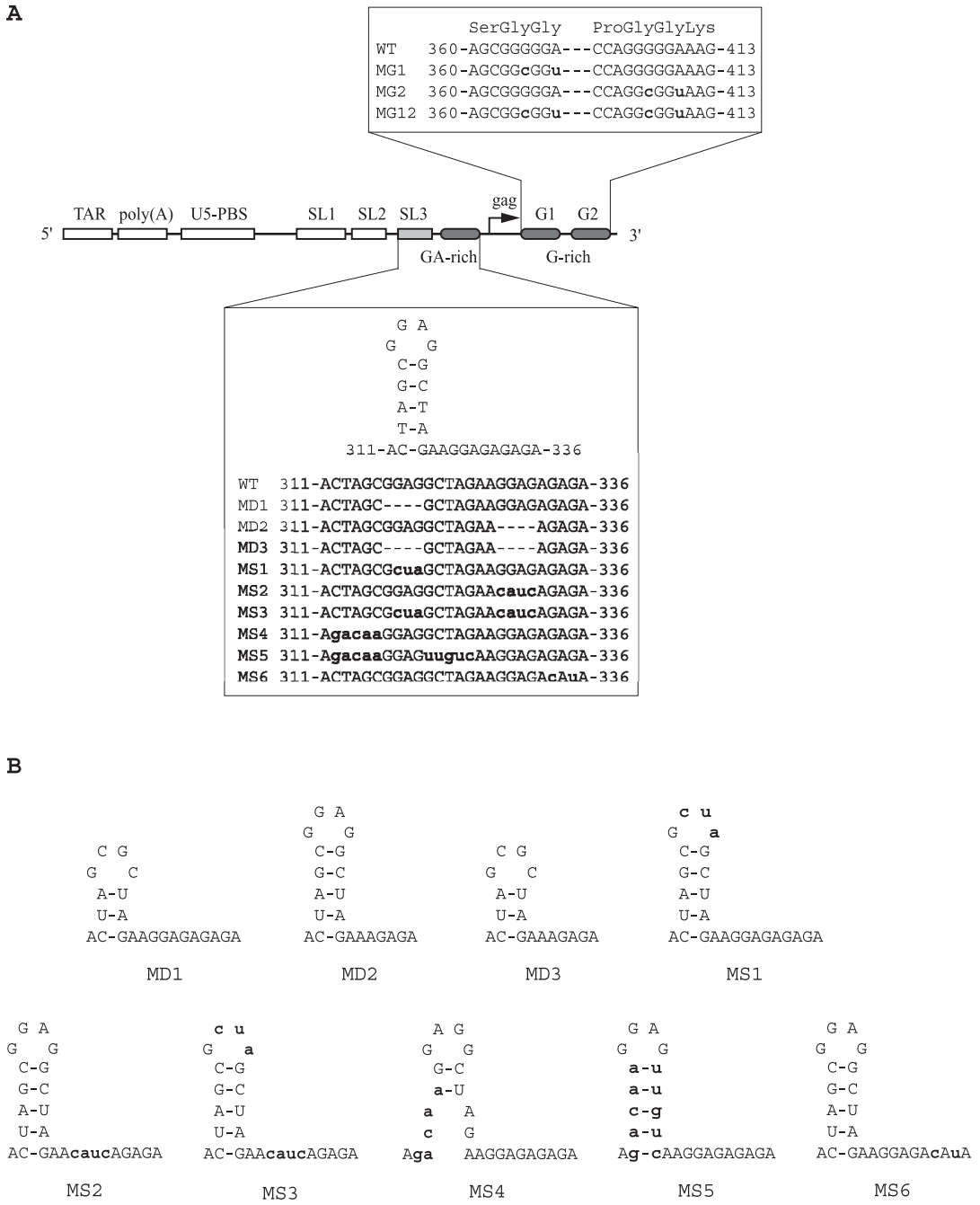

FIG. 1. Description of mutations generated in HIV-1 RNA sequences downstream of the 5′ major splice donor (SD) site. (A) Mutations MG1, MG2, and MG12 are shown at the top; these altered the G-rich sequences without changing relevant amino acid sequences in MA. Mutations in SL3 and the GA-rich region are diagrammed at the bottom. Deleted nucleotides are indicated by a dash. Nucleotides numbers refer to the first nucleotide of the R region. A number of structural domains in the leader region are shown: these include TAR, poly(A), U5-PBS, SL1, SL2, and SL3. (B) Schematic representation of all mutants listed in A. In MS1, the loop sequence was changed without disrupting the SL3 stem; in MS4, the left portion of the stem sequences was replaced, destabilizing stem base pairing; in MS5, the stem in SL3 was restored by insertion of a compensatory mutation. MD1 represents a deletion of the SL3 loop; MD2 represents a deletion of the GA-rich sequence just adjacent to SL3; MD3 is a combination of the MD1 and MD2 deletions; MS2 contains a substitution of the GA-rich sequence just adjacent to SL3; MS3 carries a combination of the MS1 and MS2 substitutions; MS6 contains substitutions of the two G's at nt 332 and 334. RNA structures were predicted by the M-Fold program (29, 44).

ture in permissive cells. In order to determine the effects of these mutations on viral RNA dimerization and packaging, we analyzed virion-derived RNA on native Northern blots (Fig. 3A and B). In addition, viral RNA packaging was further investigated by RNase protection assay analysis (Fig. 3C to F). Since all of our mutations were situated in or just downstream of SL3, we designed an RNase protection assay probe that was complementary to sequences spanning the region from within

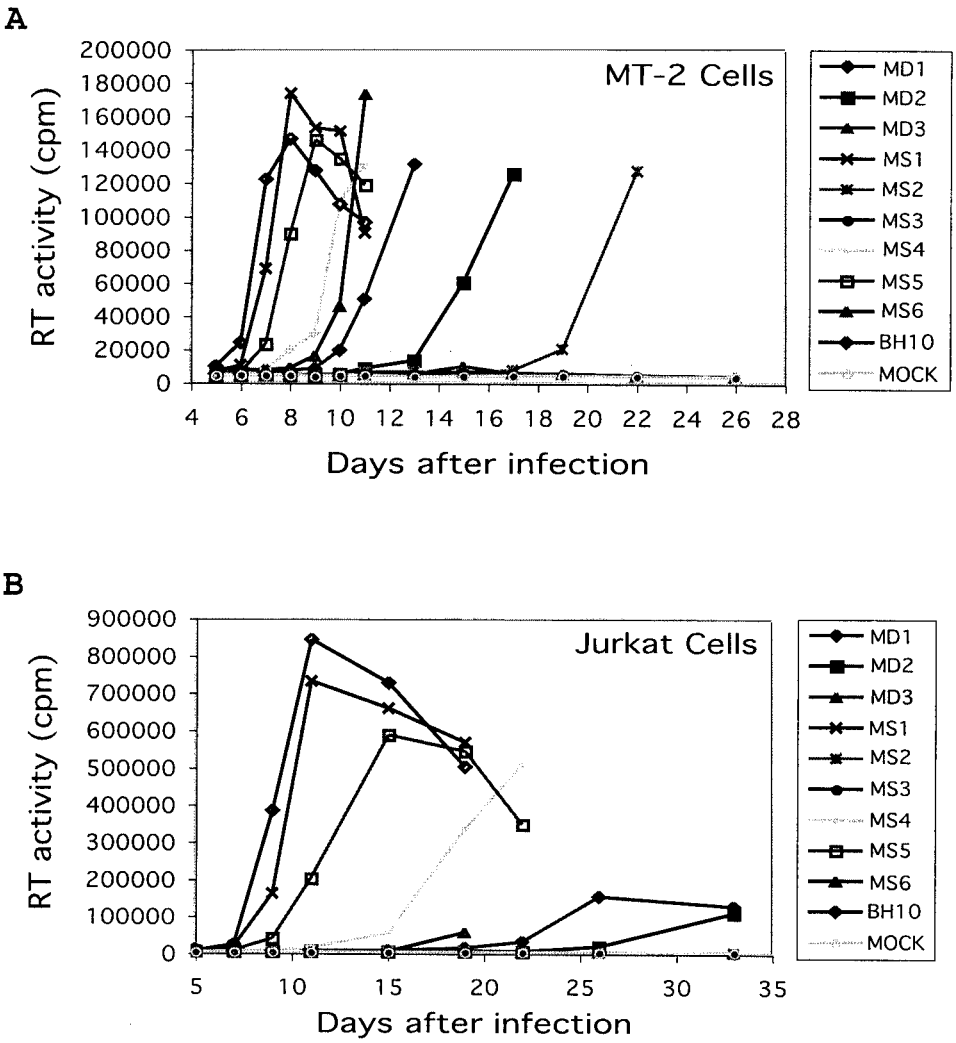

FIG. 2. Infectiousness of mutant viruses MD1 to MD3 and MS1 to MS6 in permissive cell lines. MT-2 cells (A) and Jurkat cells (B) were infected with an amount of progeny virus equal to 5 ng of p24 antigen. Virus growth was monitored by measuring reverse transcriptase activity in culture fluids at various times. Mock infection represents exposure of cells to heat-inactivated wild-type viruses.

U3 to just before SL3. This particular probe generates the same digestion pattern for wild-type HIV-1 RNA and each of our mutants, as depicted in Fig. 3C.

The results of these analyses demonstrate that the majority of wild-type viral RNA was present as a dimer (Fig. 3A, lane 10). In the case of construct MD1, overall levels of viral RNA were reduced compared to wild-type BH10 (Fig. 3A, lane 1 versus lane 11, and Fig. 3D and F), and more than 50% of the viral RNA migrated as monomers (Fig. 3A, lane 1, and Fig. 3B). However, substitution of the SL3 loop sequence in MS1 did not affect either RNA dimerization or packaging (Fig. 3A and D, lane 4; Fig. 3B and F), suggesting that the loop sequence itself is not required for either of these activities.

The negative effect of the MD1 mutation on RNA dimerization and packaging may be due to destabilization of the SL3 secondary structure. To address this issue, the base pairing of the stem structure was disrupted by the MS4 mutation (Fig. 1B), and the results show that this led to a decrease in overall levels of both viral RNA and dimeric RNA (Fig. 3A and D, lane 7; Fig. 3B and F). Restoration of the base pairing in the stem structure by a compensatory mutation in MS5 (Fig. 1B) corrected these defects (Fig. 3A and D, lane 8; Fig. 3B and F). Therefore, SL3 not only acts as a packaging signal but also affects RNA dimerization, and SL3 secondary structure must play a major role in each of these activities.

The wild-type and mutant proviral constructs produced similar amounts of viral RNA within the cytoplasm (Fig. 3E), with the exception of MS2 (lane 5), which may have been due to a difference in transfection efficiency. Analysis of the viral RNA expressed within the cells revealed that all mutants tested generated approximately twice as much genomic as spliced viral RNA transcripts. As for viral RNA encapsidated into virions, wild-type HIV-1 packaged genomic RNA almost exclusively, while all mutants encapsidated detectable levels of spliced RNA. Therefore, SL3 and the downstream region play important roles in the specific packaging of full-length genomic RNA, with concomitant exclusion of the spliced RNA. This observation is consistent with a previous report on this subject (7).

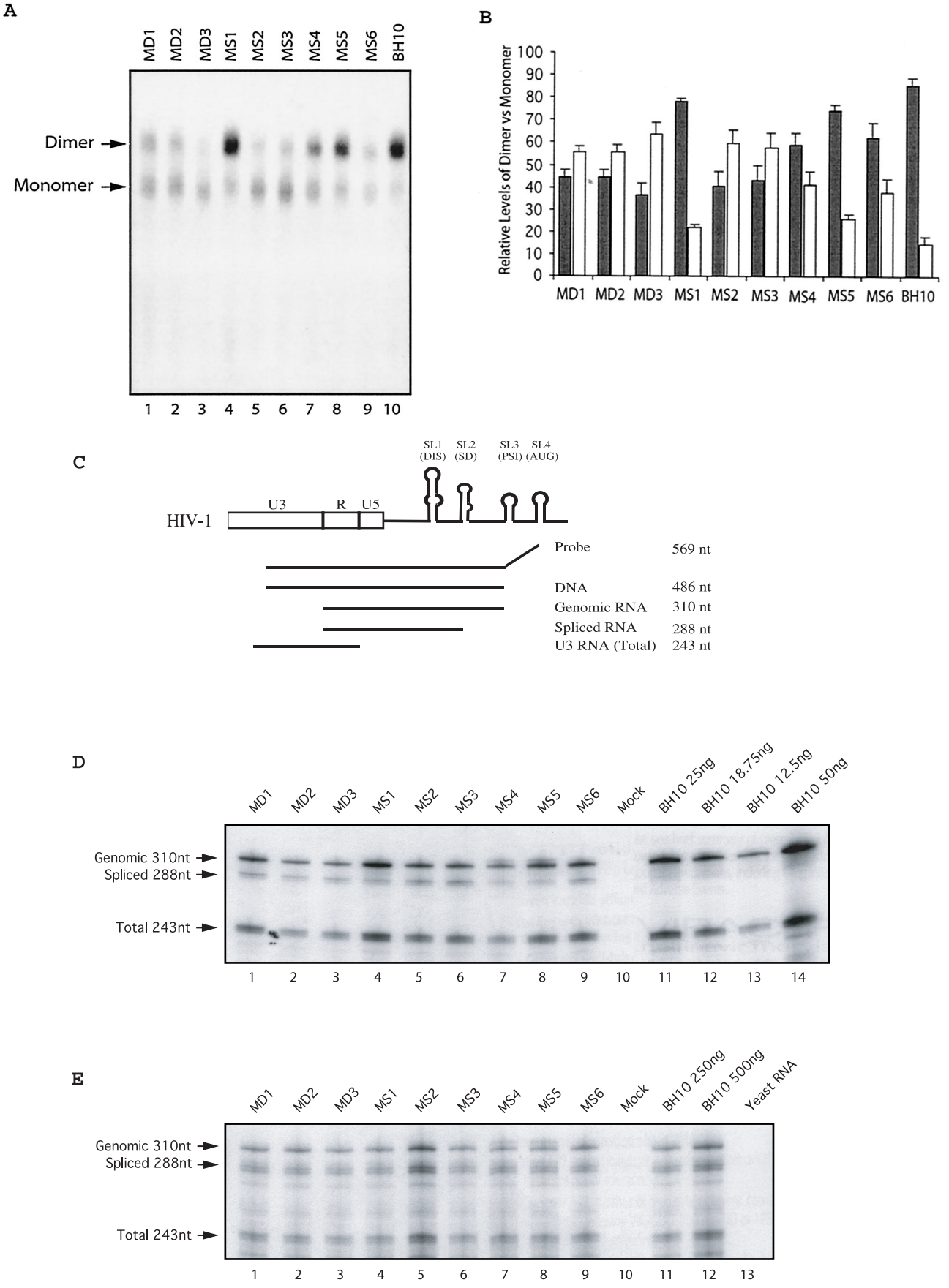
A
MD1 MD2 MD3 MS1 MS2 MS3 MS4 MS5 MS6 BH10
Dimer
Monomer
1 2 3 4 5 6 7 8 9 10
B
Relative Levels of Dimer vs Monomer
100 90 80 70 60 50 40 30 20 10 0
MD1 MD2 MD3 MS1 MS2 MS3 MS4 MS5 MS6 BH10
C
SL1 (DIS) SL2 (SD) SL3 (PSI) SL4 (AUG)
HIV-1
U3 R U5
Probe 569 nt
DNA 486 nt
Genomic RNA 310 nt
Spliced RNA 288 nt
U3 RNA (Total) 243 nt
D
MD1 MD2 MD3 MS1 MS2 MS3 MS4 MS5 MS6 Mock BH10 25ng BH10 18.75ng BH10 12.5ng BH10 50ng
Genomic 310nt
Spliced 288nt
Total 243nt
1 2 3 4 5 6 7 8 9 10 11 12 13 14
E
MD1 MD2 MD3 MS1 MS2 MS3 MS4 MS5 MS6 Mock BH10 250ng BH10 500ng Yeast RNA
Genomic 310nt
Spliced 288nt
Total 243nt
1 2 3 4 5 6 7 8 9 10 11 12 13

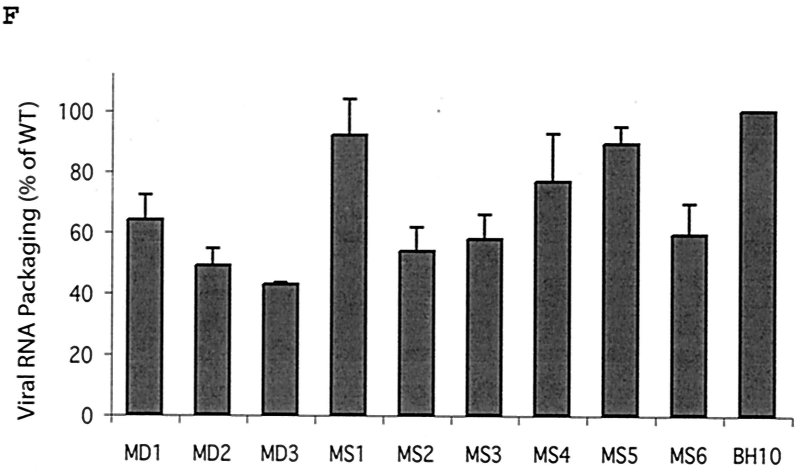

FIG. 3. Effects of various mutations on viral RNA dimerization and packaging. (A) Viral RNA was prepared from mutant viruses MD1 to MD3 and MS1 to MS6 (lanes 1 to 9) and wild-type virus BH10 (lane 10), equivalent to 150 ng of p24 antigen, and fractionated on native agarose gels, followed by Northern blot analysis. Dimers and monomers are indicated on the left side of the gels. Results from one representative gel are shown. (B) Band intensities of dimer (solid bars) and monomer (open bars) signals were measured with the NIH Image program, and relative levels for each construct were plotted. The results represent pooled data from three Northern blots with virion-derived RNA from three independent transfections of each mutant. (C) Schematic illustration of the RNase protection assay system used to quantify viral RNA, based on the strategy used by Clever and Parslow (7). Shown are the 5′ long terminal repeat sequences, including U3, R, U5, and stem loops 1 to 4. Below are shown the probe (569 nt) and the protected fragments that would be generated from the various viral RNA and DNA sequences; these include DNA (486 nt); full-length genomic RNA (310 nt; panel D, upper band), spliced RNA (288 nt; panel D, middle band), and 3′ long terminal repeat sequence (243 nt; panel D, lower band), which serves as an internal control for total viral RNA. (D) RNase protection assay performed on virion-derived RNA from mutants MD1 to MD3 and MS1 to MS6 (lanes 1 to 9) and wild-type BH10 (lane 11) viruses. An amount of viral RNA equivalent to 25 ng of p24 capsid antigen was annealed to 10^5 cpm of radiolabeled riboprobe and digested with RNases specific for single-stranded RNA, and protected fragments were separated by denaturing 5% polyacrylamide gel electrophoresis. Transfection of the pSP72 cloning vector served as a mock experiment (lane 10). A dilution series of wild-type RNA was analyzed to show the linear range of the assay (25, 18.75, and 12.5 ng of p24 in lanes 11 to 13, respectively). Wild-type RNA equivalent to 50 ng of p24 was also analyzed to demonstrate that the assay was not saturated at 25 ng of p24 (lane 14). One representative gel is shown from two independent experiments. (E) RNase protection assay performed on cytoplasmic RNA from transfections of mutants MD1 to MD3 and MS1 to MS6 (lanes 1 to 9) and wild-type BH10 (lane 11) DNA constructs as described for D with 250 ng of RNA. A twofold sample (500 ng) of cytoplasmic RNA from transfection of wild type BH10 was analyzed to demonstrate that the assay was not saturated at 250 ng of RNA (lane 12). A sample containing 10 μg of yeast tRNA was used as a negative control (lane 13). One representative gel is shown from two independent experiments. (F) Packaging levels of mutant viral RNA expressed as a percentage of that of wild-type (WT) virus BH10 (arbitrarily set at 100%). The bar graph represents data pooled from three Northern blots and two RNase protection assay gels with RNA from five independent transfections of each mutant.

We then compared the thermostability of the mutant and wild-type RNA dimers by incubating RNA samples at different temperatures before separation on native agarose gels. The results show that wild-type viral RNA dimers began to dissociate at 50°C and were completely converted to monomers at 55°C (Fig. 4). Similar results were obtained with RNA samples containing any of the MD1, MS1, MS4, and MS5 mutations (Fig. 4). Apparently, RNA dimers within these mutant virus particles displayed thermostability similar to that of the wild-type RNA dimers. Our mutant viruses can be ranked as MS1 > MS5 > MS4 > MD1 on the basis of overall RNA levels, dimer levels within virions, and infectivity (summarized in Table 1).

Since we were interested in studying the effects of our mutations on viral RNA dimerization as well as packaging, various amounts of viral RNA were loaded onto native Northern blots based on equivalent amounts of virus. However, some of our mutants displayed packaging defects; thus, smaller amounts of viral RNA from these mutants were assessed by Northern blotting than for wild-type virus. In order to test the possibility that the dimerization defects seen in our mutants might indirectly result from a lower RNA concentration, we performed a Northern blot analysis of RNA from one mutant which showed a packaging defect (MD1), along with wild-type BH10 RNA.

We loaded a series of diluted viral RNA samples equivalent to 300, 200, 100, and 50 ng of p24. The results show that the dimer-monomer ratios for neither MD1 nor wild-type viral RNA were affected by decreasing the amount of RNA loaded in the well; approximately 85 to 90% of wild-type RNA was present as dimers regardless of the quantity of viral RNA employed (Fig. 5). A comparison of lanes 2 and 7 in Fig. 5A also shows that an increase in the amount of mutant RNA did not enhance RNA dimer levels. Thus, the dimerization defects seen on our gels are not an indirect result of RNA concentrations.

Mutations in GA-rich RNA sequences at nt 325 to 336 significantly reduce levels of both viral RNA dimerization and packaging. Previous findings have shown that a GA-rich RNA sequence downstream of the SL3 structure participates in viral RNA packaging (1, 6, 25). To assess the role of this RNA sequence in viral RNA dimerization, we either deleted the 4 nt, 5′-GGAG-3′ (nt 327 to 330), in construct MD2 or changed them to 5′-CATC-3′ in construct MS2 (Fig. 1). The results of infection assays showed that both mutations markedly decreased viral replication capacity in both MT-2 and Jurkat cells, with MS2 displaying the greater effect of the two (Fig. 2); this is potentially attributable to the fact that the mutation in MS2, unlike that of MD2, inserted C and T bases as well as

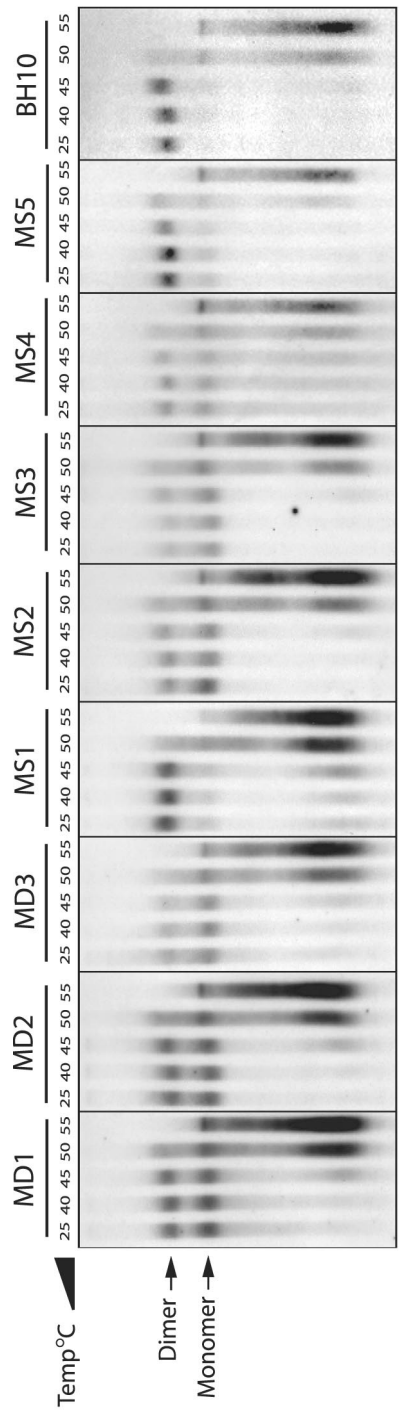

FIG. 4. Measurement of RNA dimer stability. Virion-derived RNA was treated at different temperatures before electrophoresis on native agarose gels. Lanes 1 to 5 represent incubations performed at 25°C, 40°C, 45°C, 50°C, and 55°C, respectively.

TABLE 1. Effects of various mutations on viral RNA packaging and dimerization as well as viral replication

Virus	% Dimers[a]	% Packaging[b]	Replication[c]
MD1	45 ± 3	68 ± 11	+++
MD2	44 ± 3	49 ± 6	++
MD3	36 ± 5	51 ± 8	+
MS1	78 ± 1	87 ± 11	++++
MS2	41 ± 6	58 ± 11	++
MS3	43 ± 7	60 ± 8	+
MS4	59 ± 6	75 ± 10	+++
MS5	74 ± 2	79 ± 8	++++
MS6	62 ± 6	61 ± 11	+
MS7	66	49	ND[d]
BH-GA	47 ± 11	63 ± 8	ND
MG1	79 ± 6	80 ± 10	++++
MG2	87 ± 1	91 ± 12	++++
MG12	84 ± 3	91 ± 9	++++
BH10	88 ± 3	100	++++

[a] Percentage of dimerized viral RNA relative to total amount of viral RNA as determined by native Northern blotting. All values represent means ± standard error for at least three independent experiments except for MS7, which includes data from two experiments.
[b] Viral RNA packaged, expressed as a percentage of that of wild-type BH10.
[c] Replication capacity was scored based on infection studies performed in MT-2 and Jurkat cells.
[d] ND, not determined.

removing G's and A's, thus diminishing the overall GA content more effectively (Fig. 1). Both MD2 and MS2 reduced viral infectivity to lower levels than did either the MD1 or MS4 mutation in SL3 (Fig. 2).

We next assessed viral RNA packaging and dimerization in the MD2 and MS2 mutant viruses and found that both displayed significant reductions in levels of viral genomic RNA (Fig. 3D, lanes 2 and 5, and Fig. 3F). Over 50% of the viral RNA present in MD2 viruses existed as monomers, as did 60% of MS2 viral RNA (Fig. 3A, lanes 2 and 5, and Fig. 3B). When RNA samples were heated at different temperatures before analysis on native agarose gels, mutant RNA dimers of MD2 and MS2 dissociated at approximately 50°C, as did wild-type RNA (Fig. 4).

To further evaluate the role of the GA-rich sequence (nt 325 to 336) in RNA dimerization, two G's at nt positions 332 and 334 were replaced in construct MS6 (Fig. 1). MS6 resulted in diminished viral infectivity in both MT-2 and Jurkat cells (Fig. 2) as well as significant reductions in RNA dimerization (Fig. 3A, lane 9, and Fig. 3B) and packaging (Fig. 3D, lane 9, and Fig. 3F), as shown by native Northern blotting and the RNase protection assay, respectively. The results of these experiments are summarized in Table 1. Thus, the GA-rich sequence at nt 325 to 336 is required for efficient viral RNA dimerization and packaging.

Additive effects of SL3 and GA-rich sequences on viral RNA packaging and dimerization. We next mutated both SL3 and the GA-rich sequences by either combining the MD1 and MD2 deletions in construct MD3 or recombining the MS1 and MS2 mutations in construct MS3 (Fig. 1). The MD3 deletion caused a further decrease in viral infectivity in comparison with either MD1 or MD2 (Fig. 2); similar observations were made with the MS3 mutant virus (Fig. 2). When virion-derived RNA samples were examined on native Northern blots, both the proportions of RNA dimers and overall levels of viral RNA in the MD3

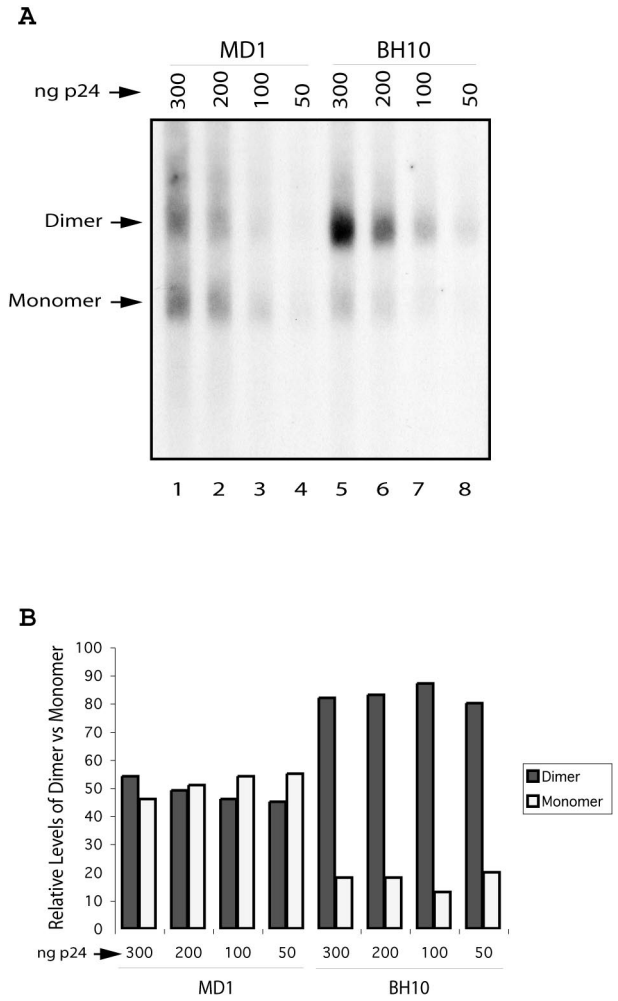

FIG. 5. Effects of RNA concentration on viral RNA dimerization. (A) A series of RNA samples of the MD1 mutant containing 300, 200, 100, and 50 ng of p24 equivalent (lanes 1 to 4) and wild-type BH10 (lanes 5 to 8) virus RNA were analyzed by native Northern blotting. Dimers and monomers are indicated on the left side of the gels. (B) Band intensities of dimer and monomer signals were measured with the NIH Image program, and relative levels for each lane were plotted.

mutant were shown to be lower than those observed in either MD1 or MD2 (Fig. 3A and D, lane 3 versus 1 and 2, and Fig. 3B and F). Thus, both SL3 and the GA-rich region must contribute independently to viral RNA dimerization and packaging. Combination of the MS1 and MS2 substitutions in MS3 caused reductions in RNA dimerization and packaging similar to those observed in MS2 (Fig. 3A and D, lane 6 versus 5, and Fig. 3B and F), presumably because MS1 did not affect RNA dimerization or packaging (Fig. 3A and D, lane 4, and Fig. 3B and F) (see Table 1 for summary). Viral RNA dimers from the MD3 and MS3 viruses dissociated at approximately 50°C, similar to wild-type RNA dimers (Fig. 4).

Mutation of CU repeats at nt 227 to 233 results in diminished levels of RNA dimerization and packaging. Our data suggest that secondary structure rather than specific SL3 RNA sequences is required for dimerization and packaging. Computer modeling studies have also predicted that the GA-rich region binds to a segment of CU repeats at nt 227 to 233 (Fig. 6A) (14) and that the SL1, SL2, and SL3 RNA motifs exist as independent domains (referred to as stems II, III, and IV in reference 14). To test whether the defective RNA packaging and dimerization that were caused by mutations in the GA-rich region resulted from destabilization of RNA-RNA interactions in this region, we replaced the CU repeats at this site with the sequence 5′-AGAG-3′ to generate construct BH-GA (Fig. 6A) (24). The results of native Northern blot analysis showed that BH-GA contained reduced levels of viral RNA (Fig. 6D) as well as a diminished proportion of dimerized RNA (Fig. 6B, lane 1, and Fig. 6C), suggesting that RNA-RNA interactions between the CU repeats (nt 227 to 233) and the GA-rich sequences (nt 325 to 336) might be important for both viral RNA packaging and dimerization.

To further understand the potential interactions between the CU repeats (nt 227 to 233) and the GA-rich sequences (nt 325 to 336) and the importance of their interactions in viral RNA packaging and dimerization, we analyzed the local secondary structure with the M-Fold algorithm (29, 44). We found that both the BH-GA and the MS6 mutations disrupted predicted base-paring between these sequences, but we were unable to design satisfactory compensatory mutations for the BH-GA mutant that would restore local base pairing in this region, possibly because of the relatively large number of nucleotides changed in BH-GA. However, we were able to restore putative stem base pairing by mutating the two C's at nt 223 and nt 225 to a G and an A, respectively, in the context of the MS6 mutation (Fig. 7A and B). This newly generated mutation was termed MS7. Surprisingly, native Northern blotting showed that the viral RNA dimerization defect was not corrected despite the predicted restoration of base pairing to a wild-type pattern (Fig. 7C, lane 2 versus 1, and Fig. 7D). Similarly, the packaging defect seen with the MS6 mutant was not overcome by the restoration of base pairing in this region in MS7 (Fig. 7E). Data regarding these mutants are summarized in Table 1. It is likely that both the CU repeats and the GA-rich sequences are important for viral RNA packaging and dimerization, but not necessarily through a direct base pairing interaction.

Mutations in two stretches of G-rich sequences affect neither viral replication nor viral RNA dimerization. Previous studies suggested that two stretches of G-rich sequences at nt 363 to 367 and nt 405 to 409 contributed to viral RNA dimerization through formation of G-tetrad structures (2, 27, 42). To determine whether these two RNA segments are involved in genomic RNA dimerization, they were either individually mutated in constructs MG1 and MG2 or simultaneously changed in construct MG12 (Fig. 1A). The substituted nucleotides were designed so that relevant amino acids in MA were not altered. None of the three mutations affected viral growth in either MT-2 or Jurkat cells (Fig. 8). In addition, wild-type levels of dimerized RNA were present in each of the MG1, MG2, and MG12 mutant viruses (Fig. 9 and Table 1). Therefore, the G-rich features of the RNA segments studied are not important for either viral replication, RNA dimerization, or packaging.

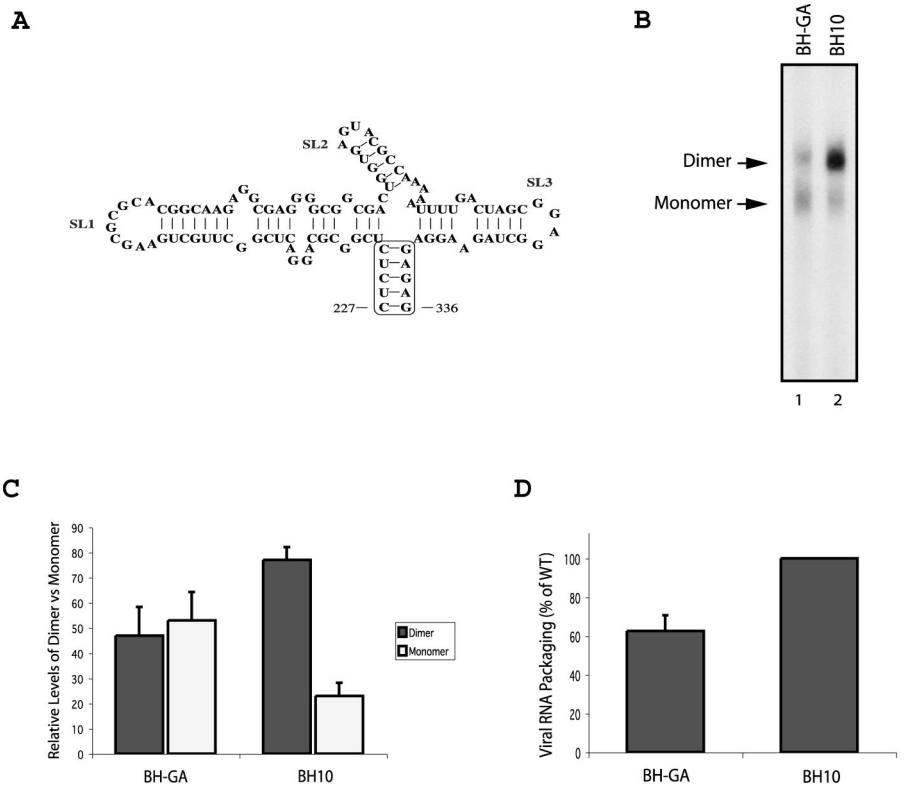

FIG. 6. Mutation of CU repeat RNA sequence (nt 227 to 233) affects viral RNA dimerization and packaging. (A) Illustration of a structural domain formed by viral RNA sequences from nt 227 to 335. This domain contains the SL1, SL2, and SL3 RNA motifs and is isolated from other RNA structures by a stem formed by long-range interactions between two stretches of RNA sequences at nt 227 to 231 and nt 332 to 336 (14). In the BH-GA mutation, the RNA stretch at nt 227 to 233 was replaced with the sequence 5′-AGAG-3′, which presumably disrupted the highlighted stem. (B) Native Northern blots of BH-GA (lane 1) and BH10 (lane 2) RNAs derived from an amount of virus particles equivalent to 150 ng of p24 antigen. The intensities of RNA signals were measured with the NIH Image program. Dimers and monomers are indicated on the left side of the gels. Results for one representative gel are shown. (C) Band intensities of dimer and monomer signals were measured with the NIH Image program, and relative levels for each construct were plotted. (D) RNA packaging levels were expressed as a percentage of that of the wild-type (WT) virus BH10 (arbitrarily set at 100%). Results shown in C and D represent pooled data from three Northern blots of three independent transfections of each mutant.

DISCUSSION

Although the RNA packaging activities of SL3 and GA-rich sequences (nt 325 to 336) have been reported previously (1, 5, 6, 7, 15, 25, 30), our results provide further in vivo evidence in this regard by measurements of viral RNA levels in the mutant viruses MD1 to MD3 and MS1 to MS6 (Fig. 3). The data from our BH-GA, MS6, and MS7 mutant viruses (Fig. 6 and 7) further demonstrate that this GA-rich RNA segment is important in the regulation of viral RNA packaging but that its packaging activity may not depend on its interaction with a stretch of CU repeats at nt 227 to 233. More importantly, our native Northern blotting results suggest that both SL3 and GA-rich sequences are required for efficient RNA dimerization (Fig. 3A and B, 6B and C, and 7C and D).

Of the four SL3 mutations studied, MD1 and MS4 caused a destabilization of SL3 structure and diminished levels of RNA dimerization; in contrast, MS1 and MS5 preserved SL3 structure and both maintained nearly wild-type levels of dimerization (Fig. 3A and B). These findings are consistent with other data showing that disruption of the SL1 stem led to aberrant RNA dimerization and that restoration of the stem structure by compensatory mutations increased RNA dimerization to wild-type levels (7, 9). Therefore, intact secondary structures of both SL1 and SL3 are needed for efficient viral RNA dimerization. Of these two RNA motifs, SL1 possesses a palindrome in the loop, the alteration of which affects RNA dimerization (9, 34, 41). In contrast, replacement of the SL3 loop sequence did not interfere with viral RNA dimerization as long as the changes did not disrupt the SL3 secondary structure (Fig. 3A and B). SL1 apparently regulates viral RNA dimerization through its loop palindrome by a kissing-loop mechanism, while SL3 affects dimerization in a manner that is independent of the loop sequence.

SL3 shows high affinity for the HIV-1 Gag and NC proteins (8). A nuclear magnetic resonance structure of a complex formed by NC and SL3 has recently been resolved and revealed specific interactions between these two molecules (10). We speculate that these specific RNA-protein interactions, thought to guide viral RNA packaging, may also be responsible for the role of SL3 in RNA dimerization.

We have shown that decreases in both RNA packaging and dimerization are the result of mutations in the SL3 and GA-

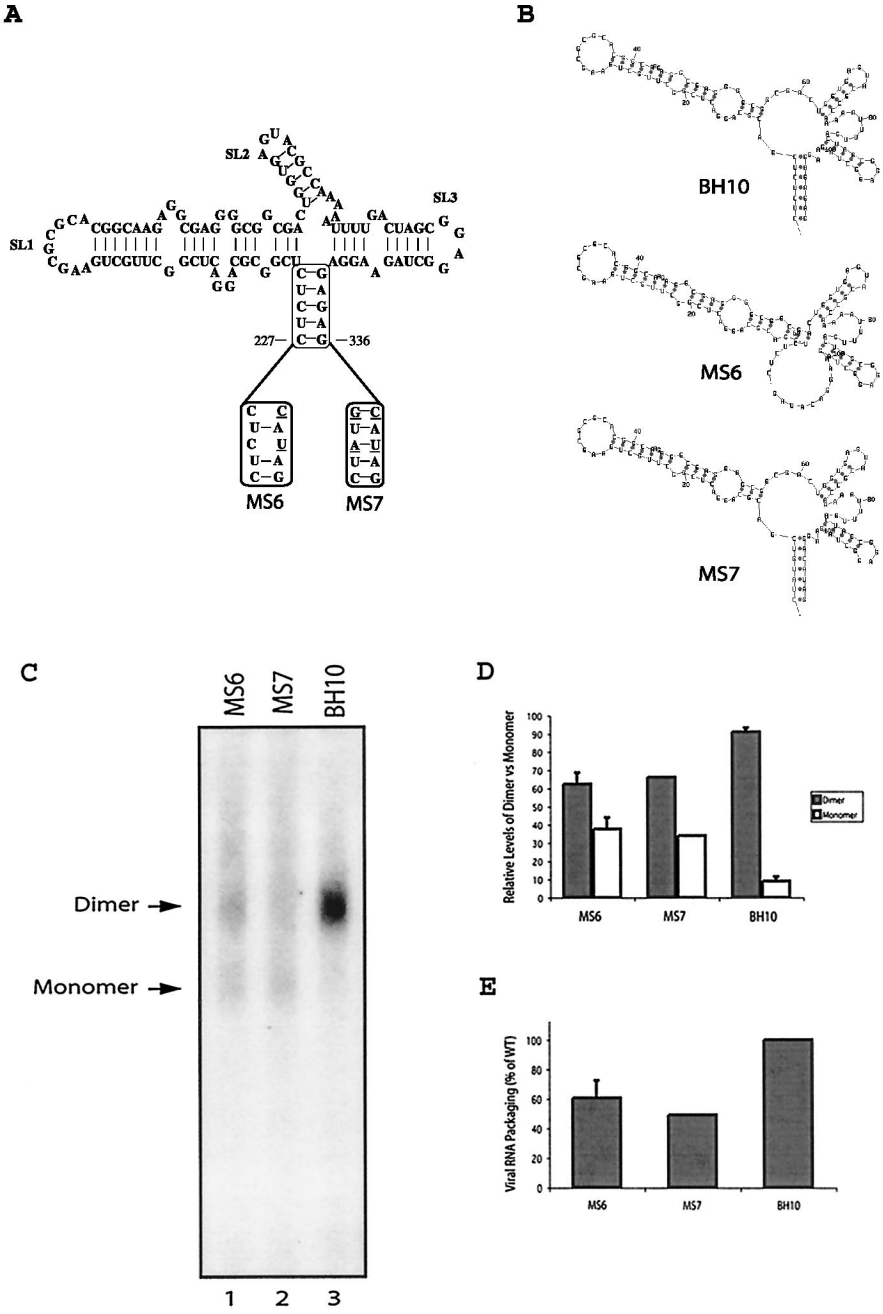

FIG. 7. Analysis of the putative RNA-RNA interactions between the CU repeats (nt 227 to 233) and the GA-rich sequences (nt 325 to 336). (A) Illustration of a structural domain formed by viral RNA sequences from nt 227 to nt 336. Nucleotides changed in MS6 and MS7 are underlined. (B) Secondary-structure models representing the region shown in A for MS6, MS7, and wild-type BH10 based on the M-Fold algorithm (29, 44). (C) Native Northern blots of MS6, MS7, and BH10 (lanes 1 to 3) RNAs derived from an amount of virus particles equivalent to 150 ng of p24 antigen. The intensities of RNA signals were measured with the NIH Image program. Dimers and monomers are indicated on the left side of the gels. Results from one representative gel are shown. (D) Band intensities of dimer and monomer signals were measured with the NIH Image program, and relative levels for each construct were plotted. (E) RNA packaging levels were expressed as a percentage of that of wild-type (WT) virus BH10 (arbitrarily set at 100%). Results shown in D and E represent pooled data from three independent experiments for MS6 and BH10 and two for MS7.

rich regions (Fig. 3, 6, and 7), but it is uncertain which of these processes is affected first. From a temporal perspective, studies with protease-negative HIV-1 suggested that viral RNA is packaged as immature dimers (11), although this may not be true for other retroviruses, such as avian leukosis virus (33). Interestingly, HIV-1 RNA may also be efficiently encapsidated in monomeric form, based on the following observations: (i) less extensive mutations of the SL1 loop (i.e., a G-loop mutation) did not affect the viral RNA content but impaired RNA dimerization. (7); (ii) compensatory mutations in Gag proteins

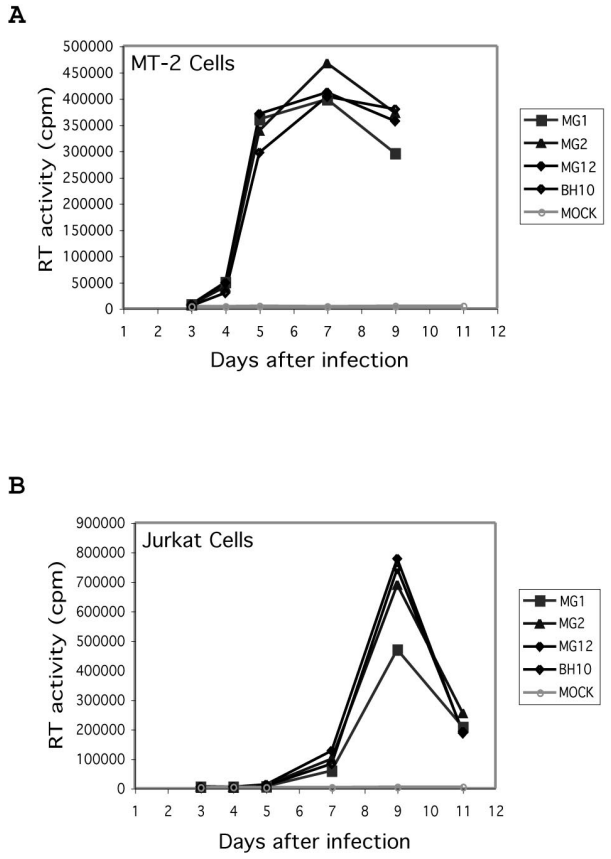

FIG. 8. Effects of MG1, MG2, and MG12 mutations on viral replication as determined by infection of MT-2 cells (A) and Jurkat cells (B). Virus growth was monitored by measurement of reverse transcriptase activity in culture fluids at various times.

(MP2 and MNC substitutions) restored viral replication and viral RNA packaging to nearly wild-type levels but did not correct defective viral RNA dimerization that was caused by deletion of the dimerization initiation site (40); (iii) mutated viruses carrying a duplicated dimerization initiation site contained wild-type levels of viral RNA, the majority of which were present as monomers (36, 37); and (iv) alteration of Gag/Gag-Pol ratios in virions reduced viral RNA dimer stability without decreasing levels of virion RNA content (39). Therefore, wild-type RNA packaging can occur in the absence of efficient RNA dimerization.

In contrast, virus particles are able to encapsidate two copies of viral RNA despite decreased packaging efficiency. When basic amino acids that flank the zinc finger motif of NC were changed to neutral amino acids in Moloney murine leukemia virus, RNA packaging was decreased; however, the viral RNA was still mainly dimeric (16). Similar observations have been made for HIV-1 (22). Therefore, RNA packaging and dimerization can be either individually or simultaneously affected by different mutations. Further studies are needed to determine which activity is affected first in the mutant viruses described herein.

In an attempt to further understand the role of the GA-rich sequences in the dimerization and packaging processes, we performed stem disruption-restoration mutagenesis experiments with the CU repeats (nt 227 to 233) and GA-rich sequences (nt 325 to 336) to determine whether they are involved in a direct RNA-RNA interaction, as depicted in Fig. 7A. Based on our dimerization data, both of these regions are important for viral RNA packaging and dimerization. However, despite the seemingly stable secondary-structure predictions generated with the M-Fold program, our MS7 compen-

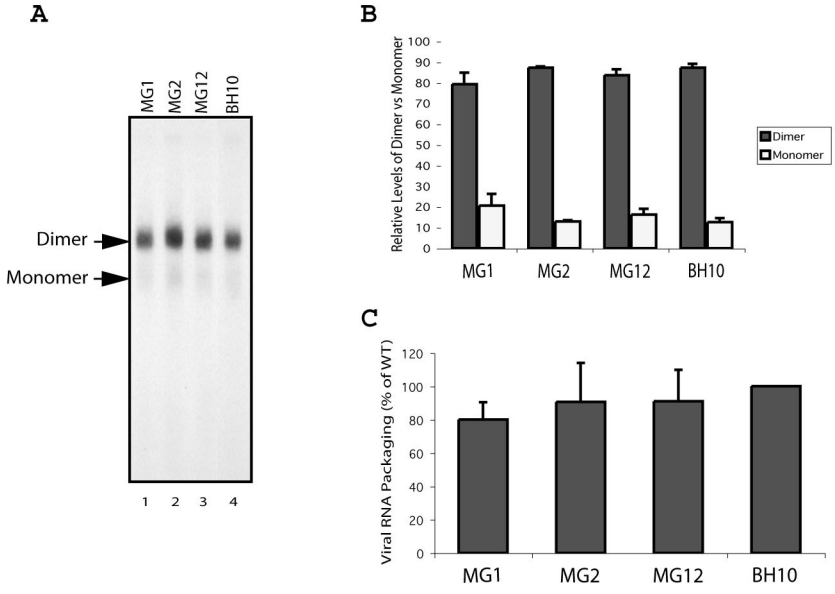

FIG. 9. Effects of MG1, MG2, and MG12 mutations on viral RNA dimerization and packaging. (A) Native Northern blot analyses were performed on MG1, MG2, and MG12 (lanes 1 to 3, respectively) and wild-type BH10 (lane 4) RNAs derived from an amount of virus particles equivalent to 150 ng of p24 antigen. The intensities of RNA signals were measured with the NIH Image program. Dimers and monomers are indicated on the left side of the gels. Results from one representative gel are shown. (B) Band intensities of dimer and monomer signals were measured with the NIH Image program, and relative levels for each construct were plotted. (C) RNA packaging levels were expressed as a percentage of that of the wild-type (WT) virus BH10 (arbitrarily set at 100%). Results shown in B and C represent pooled data from three independent experiments.

satory mutation, which would theoretically restore base pairing in this region, did not correct the packaging and dimerization defects seen with the MS6 mutant. These results suggest that the mechanism by which these sequences are involved in dimerization and packaging may not act through direct RNA-RNA interactions between these sequences.

Interactions between the CU repeats (nt 227 to 233) and GA-rich sequences (nt 325 to 336) have been proposed on the basis of computer modeling and in vitro probing experiments, in which the RNA structure thus formed was referred to as stem I (14). However, the stability of stem I was questioned, as the reactivity of G's in this region with kethoxal suggests that they are unpaired. On this basis, it was concluded that stem I may exist transiently or in equilibrium with an unpaired state. It is possible that the CU repeats (nt 227 to 233) and GA-rich sequences (nt 325 to 336) may bind to other RNA regions as well and thus regulate viral RNA dimerization and packaging. Alternatively, they may be involved in more than one type of RNA-RNA interaction. For example, recent in vitro data suggest that the HIV-1 leader RNA can form alternate structures that are proposed to regulate RNA dimer formation (4, 17). Although these models have been generated with synthetic RNA transcripts, which for the most part do not include SL3, and await in vivo confirmation, it might be interesting to consider the involvement of SL3 and/or GA-rich sequences in these conformational switches with respect to dimerization and/or packaging.

The mutations that we generated in SL3 and the GA-rich region may also have disrupted dimerization initiation site structure and indirectly affected RNA dimerization. Although structural studies of synthetic viral RNA fragments will provide insight on this topic, the putative effects of our mutations on dimerization initiation site structure can also be assessed by the M-Fold program (29, 44). We divided predicted structures representing each mutation into two groups, based on the presence or absence of the dimerization initiation site motif, and plotted ΔG values accordingly (Fig. 10). In the case of wild-type viral RNA, structures containing a dimerization initiation site are preferable due to their low ΔG values. For MS1 and MS5, in which SL3 structure was preserved, secondary structures containing a dimerization initiation site were also strongly favored. In the cases of MD1 and MS4, structures containing a dimerization initiation site tended to show ΔG values lower than those of constructs lacking a dimerization initiation site. Therefore, mutations in SL3 may have affected RNA dimerization without a corresponding influence on dimerization initiation site structure.

In contrast, the MD2, MS2, and MS6 mutations in the GA-rich region failed to yield dimerization initiation site-containing structures with favorable ΔG values (Fig. 10). This suggests that these mutations adversely impacted the formation of the dimerization initiation site structure, which, in turn, led to defective RNA dimerization and packaging. Since as few as two nucleotide alterations in MS6 can alter the dimerization initiation site structure, we believe that the more extensive GA-rich sequences at nt 325 to 336 may be essential in preserving the integrity of the HIV-1 RNA leader region and in presenting the dimerization initiation site RNA motif for dimerization.

Purine quartet structures were also proposed to play a role

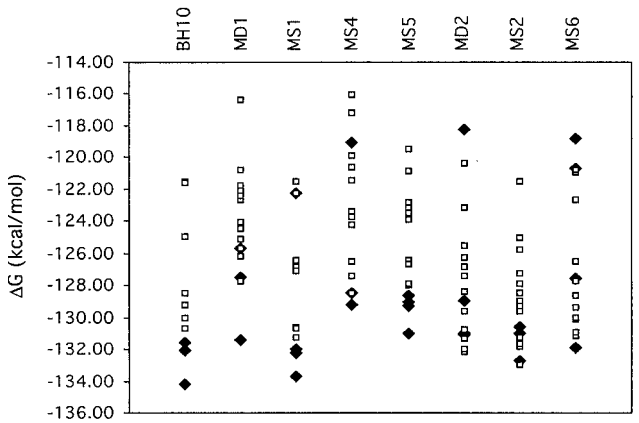

FIG. 10. Structural analysis of mutated and wild-type HIV-1 RNA sequences spanning nt 1 to 360 on the basis of the M-Fold program (29, 44). Each point in a series represents one possible structural prediction that the program generates. For sequences 300 to 400 nt in length, the program typically generates 12 to 15 possible structures and ranks them based on free-energy (ΔG) calculations. Structures representing each mutation were divided into two groups based on the presence (◆) or absence (□) of the dimerization initiation site (SL1) motif, and their ΔG values are plotted.

in RNA dimerization, as shown by in vitro studies performed with synthetic viral RNA fragments (2, 26, 42). However, virion-derived RNA dimers are not stabilized by potassium, which in general enhances purine quartet structures (11). Furthermore, interruption of the G-rich region at nt 817 to 821 in HIV-1 did not affect viral RNA dimerization (13). Finally, as shown here, mutations in two stretches of G-rich sequences did not impact viral RNA dimerization or packaging, confirming that purine quartets are not involved in these processes.

In summary, our data provide evidence for the involvement of RNA packaging signals that are located downstream of the 5′ splice donor site in HIV-1 RNA dimerization. These findings support the notion that multiple RNA elements may be needed for RNA dimerization in retroviruses, as was recently demonstrated in murine leukemia virus (26, 32). Since SL3 exhibits high affinity for NC protein, it is proposed that this RNA element may regulate HIV-1 RNA dimerization via interactions with NC.

ACKNOWLEDGMENTS

We thank Liwei Rong for helpful suggestions and Mervi Detorio and Maureen Oliveira for technical assistance.

Rodney S. Russell is a recipient of a Canadian Institutes of Health Research (CIHR) doctoral award, and Andrew J. Mouland and Chen Liang are research scholars of the Fonds pour la Recherche en Santé du Québec (FRSQ). This work was supported by grants from the CIHR.

REFERENCES

1. **Aldovini, A., and R. A. Young.** 1990. Mutations of RNA and protein sequences involved in human immunodeficiency virus type 1 packaging result in production of noninfectious virus. J. Virol. **64:**1920–1926.
2. **Awang, G., and D. Sen.** 1993. Mode of dimerization of HIV-1 genomic RNA. Biochemistry **32:**11453–11457.
3. **Berkhout, B., and J. L. van Wamel.** 1996. Role of the dimerization initiation site hairpin in replication of human immunodeficiency virus type 1. J. Virol. **70:**6723–6732.
4. **Berkhout, B., and J. L. van Wamel.** 2000. The leader of the HIV-1 RNA genome forms a compactly folded tertiary structure. RNA **6:**282–295.

5. **Berkowitz, R., J. Fisher, and S. P. Goff.** 1996. RNA packaging. Curr. Top. Microbiol. Immunol. **214:**177–218.
6. **Clavel, F., and J. M. Orenstein.** 1990. A mutant of human immunodeficiency virus with reduced RNA packaging and abnormal particle morphology. J. Virol. **64:**5230–5234.
7. **Clever, J. L., and T. G. Parslow.** 1997. Mutant human immunodeficiency virus type 1 genomes with defects in RNA dimerization or encapsidation. J. Virol. **71:**3407–3414.
8. **Clever, J., C. Sassetti, and T. G. Parslow.** 1995. RNA secondary structure and binding sites for *gag* gene products in the 5′ packaging signal of human immunodeficiency virus type 1. J. Virol. **69:**2101–2109.
9. **Clever, J. L., M. L. Wong, and T. G. Parslow.** 1996. Requirements for kissing-loop-mediated dimerization of human immunodeficiency virus RNA. J. Virol. **70:**5902–5908.
10. **De Guzman, R. N., Z. R. Wu, C. C. Stalling, L. Pappalardo, P. N. Borer, and M. F. Summers.** 1998. Structure of the HIV-1 nucleocapsid protein bound to the SL3 psi-RNA recognition element. Science **279:**384–388.
11. **Fu, W., R. J. Gorelick, and A. Rein.** 1994. Characterization of human immunodeficiency virus type 1 dimeric RNA from wild-type and protease-defective virions. J. Virol. **68:**5013–5018.
12. **Guschlbauer, W., J. F. Chantot, and D. Thiele.** 1990. Four-stranded nucleic acid structures 25 years later: from guanosine gels to telomer DNA. J. Biomol. Struct. Dyn. **8:**491–511.
13. **Haddrick, M., A. L. Lear, A. J. Cann, and S. Heaphy.** 1996. Evidence that a kissing loop structure facilitates genomic RNA dimerisation in HIV-1. J. Mol. Biol. **259:**58–68.
14. **Harrison, G. P., and A. M. Lever.** 1992. The human immunodeficiency virus type 1 packaging signal and major splice donor region have a conserved stable secondary structure. J. Virol. **66:**4144–4153.
15. **Harrison, G. P., G. Miele, E. Hunter, and A. M. Lever.** 1998. Functional analysis of the core human immunodeficiency virus type 1 packaging signal in a permissive cell line. J. Virol. **72:**5886–5896.
16. **Housset, V., H. De Rocquigny, B. P. Roques, and J.-L. Darlix.** 1993. Basic amino acids flanking the zinc finger of Moloney murine leukemia virus nucleocapsid protein NCp10 are critical for virus infectivity. J. Virol. **67:** 2537–2545.
17. **Huthoff, H., and B. Berkhout.** 2001. Two alternating structures of the HIV-1 leader RNA. RNA **7:**143–157.
18. **Kung, H. J., S. Hu, W. Bender, J. M. Bailey, N. Davidson, M. O. Nicolson, and R. M. McAllister.** 1976. RD-114, baboon, and woolly monkey viral RNA's compared in size and structure. Cell **7:**609–620.
19. **Laughrea, M., and L. Jette.** 1994. A 19-nucleotide sequence upstream of the 5′ major splice donor is part of the dimerization domain of human immunodeficiency virus 1 genomic RNA. Biochemistry **33:**13464–13474.
20. **Laughrea, M., and L. Jette.** 1996. Kissing-loop model of HIV-1 genome dimerization: HIV-1 RNAs can assume alternative dimeric forms, and all sequences upstream or downstream of hairpin 248–271 are dispensable for dimer formation. Biochemistry **35:**1589–1598.
21. **Laughrea, M., L. Jette, J. Mak, L. Kleiman, C. Liang, and M. A. Wainberg.** 1997. Mutations in the kissing-loop hairpin of human immunodeficiency virus type 1 reduce viral infectivity as well as genomic RNA packaging and dimerization. J. Virol. **71:**3397–3406.
22. **Laughrea, M., N. Shen, L. Jette, J.-L Darlix, L. Kleiman, and M. A. Wainberg.** 2001. Role of distal zinc finger of nucleocapsid protein in genomic RNA dimerization of human immunodeficiency virus type 1: no role for the palindrome crowning the R-U5 hairpin. Virology **281:**109–116.
23. **Lee, J. S., D. H. Evans, and A. R. Morgan.** 1980. Polypurine DNAs and RNAs form secondary structures which may be tetra-stranded. Nucleic Acids Res. **8:**4305–4320.
24. **Liang, C., X. Li, Y. Quan, M. Laughrea, L. Kleiman, J. Hiscott, and M. A. Wainberg.** 1997. Sequence elements downstream of the human immunodeficiency virus type 1 long terminal repeat are required for efficient viral gene transcription. J. Mol. Biol. **272:**167–177.
25. **Luban, J., and S. P. Goff.** 1994. Mutational analysis of cis-acting packaging signals in human immunodeficiency virus type 1 RNA. J. Virol. **68:**3784–3793.
26. **Ly, H., and T. G. Parslow.** 2002. Bipartite signal for genomic RNA dimerization in Moloney murine leukemia virus. J. Virol. **76:**3135–3144.
27. **Marquet, R., F. Baudin, C. Gabus, J.-L. Darlix, M. Mougel, C. Ehresmann, and B. Ehresmann.** 1991. Dimerization of human immunodeficiency virus (type 1) RNA: stimulation by cations and possible mechanism. Nucleic Acids Res. **19:**2349–2357.
28. **Marquet, R., J. C. Paillart, E. Skripkin, C. Ehresmann, and B. Ehresmann.** 1994. Dimerization of human immunodeficiency virus type 1 RNA involves sequences located upstream of the splice donor site. Nucleic Acids Res. **22:**145–151.
29. **Mathews, D. H., J. Sabina, M. Zuker, and D. H. Turner.** 1999. Expanded sequence dependence of thermodynamic parameters improves prediction of RNA secondary structure. J. Mol. Biol. **288:**911–940.
30. **McBride, M. S., and A. T. Panganiban.** 1997. Position dependence of functional hairpins important for human immunodeficiency virus type 1 RNA encapsidation in vivo. J. Virol. **71:**2050–2058.
31. **Muriaux, D., P. Fosse, and J. Paoletti.** 1996. A kissing complex together with a stable dimer is involved in the HIV-1Lai RNA dimerization process in vitro. Biochemistry **35:**5075–5082.
32. **Oroudjev, E. M., P. C. Kang, and L. A. Kohlstaedt.** 1999. An additional dimer linkage structure in Moloney murine leukemia virus RNA. J. Mol. Biol. **291:**603–613.
33. **Ortiz-Conde, B. A., and S. H. Hughes.** 1999. Studies of the genomic RNA of leukosis viruses: implications for RNA dimerization. J. Virol. **73:**7165–7174.
34. **Paillart, J. C., E. Skripkin, B. Ehresmann, C. Ehresmann, and R. Marquet.** 1996. A loop-loop "kissing" complex is the essential part of the dimer linkage of genomic HIV-1 RNA. Proc. Natl. Acad. Sci. USA **93:**5572–5577.
35. **Sakuragi, J. I., and A. T. Panganiban.** 1997. Human immunodeficiency virus type 1 RNA outside the primary encapsidation and dimer linkage region affects RNA dimer stability in vivo. J. Virol. **71:**3250–3254.
36. **Sakuragi, J., T. Shioda, and A. T. Panganiban.** 2001. Duplication of the primary encapsidation and dimer linkage region of human immunodeficiency virus type 1 RNA results in the appearance of monomeric RNA in virions. J. Virol. **75:**2557–2565.
37. **Sakuragi, J., A. Iwamoto, and T. Shioda.** 2002. Dissociation of genome dimerization from packaging functions and virion maturation of human immunodeficiency virus type 1. J. Virol. 76, 959–967.
38. **Sambrook, J., E. F. Fritsch, and T. Maniatis.** 1989. Molecular cloning: a laboratory manual, 2nd ed. Cold Spring Harbor Laboratory Press, Cold Spring Harbor, N.Y.
39. **Shehu-Xhilaga, M., S. M. Crowe, and J. Mak.** 2001. Maintenance of the Gag/Gag-Pol ratio is important for human immunodeficiency virus type 1 RNA dimerization and viral infectivity. J. Virol. **75:**1834–1841.
40. **Shen, N., L. Jette, C. Liang, M. A. Wainberg, and M. Laughrea.** 2000. Impact of human immunodeficiency virus type 1 RNA dimerization on viral infectivity and of stem-loop B on RNA dimerization and reverse transcription and dissociation of dimerization from packaging. J. Virol. **74:**5729–5735.
41. **Skripkin, E., J. C. Paillart, R. Marquet, B. Ehresmann, and C. Ehresmann.** 1994. Identification of the primary site of the human immunodeficiency virus type 1 RNA dimerization in vitro. Proc. Natl. Acad. Sci. USA **91:**4945–4949.
42. **Sundquist, W. I., and S. Heaphy.** 1993. Evidence for interstrand quadruplex formation in the dimerization of human immunodeficiency virus 1 genomic RNA. Proc. Natl. Acad. Sci. USA **90:**3393–3397.
43. **Zhang, S., H. Hara, H. Kaji, and A. Kaji.** 1997. Inhibition of HIV type 1 RNA dimerization by antisense DNA corresponding to the 17-nucleotide sequence downstream from the splice donor site of HIV type 1 RNA. AIDS. Res. Hum. Retrovir. **13:**865–873.
44. **Zuker, M., D. H. Mathews, and D. H. Turner.** 1999. Algorithms and thermodynamics for RNA secondary structure prediction: a practical guide, p. 11–43. *In* J. Barciszewski and B. F. C. Clark (ed.), RNA biochemistry and biotechnology. Kluwer Academic Publishers, Dordrecht, The Netherlands.